Galileo Comes to the Surface!

de Hosson, J.T.M.; Cavaleiro, A.

Published in:
Nanostructured Coatings

Publication date:
2006

1

Galileo Comes to the Surface!

Jeff T. M. De Hosson[1] and Albano Cavaleiro[2]

[1]Department of Applied Physics, Materials Science Centre and the Netherlands Institute for Metals Research, University of Groningen, Nijenborgh 4, 9747 A. G. Groningen, The Netherlands

[2]Departamento de Engenharia Mecanica, FCTUC, Universidade de Coimbra Pinhal de Marrocos, 3030 Coimbra, Portugal

1. INTRODUCTION

The year was 1635: Galileo completed his "Dialogues concerning *new* sciences."[1] The science listed first was his study of "*what holds solids together*?" and "*why do they fall apart*?" It is fair to say that since his "Dialogues," the former question has developed to the core of interests in condensed matter physics, whereas the latter became an important branch of engineering. After the introduction of quantum mechanics, about 300 years later, the question "what holds solids together?" became based on collective excitations. These concepts were very successful in explaining functional properties of materials. In contrast, a similar success was not achieved in explaining the mechanical properties and the second question of Galileo, namely "why do solids fall apart?" could not be properly answered. Mechanical properties are determined by the collective behavior of defects rather than by the bonding between atoms and electrons. Even the behavior of one singular defect is often irrelevant. For instance, there exists a vast amount of microscopy analyses on *ex situ* deformed solids that try to link observed defect patterns to the mechanical behavior characterized by stress–strain curves. However, in spite of the enormous effort that has been put in both theoretical and experimental works, a clear physical picture that could even predict one stress–strain curve and failure by crack propagation of a coating is still lacking. The reason is quite obvious: in plastic deformation and in fracture we are faced with very nonlinear effects. These phenomena are irreversible and far from equilibrium and consequently cannot be treated by common solid-state physics approaches. As a result, this area of research has largely been ignored by condensed matter physics. The problem was too tough to be "cracked,"

so to speak. However, like in all sciences, he who would eat the kernel must crack the nut.

Luckily enough the tide is turning for two reasons. The first reason lies in new instrumental developments, which permit microstructural control on a nanometer scale, often by sophisticated processing. Alongside these developments in processing, it became possible to do *in situ* mechanical experiments under controlled conditions in conjunction with microscopy analyses, for both structural and chemical information. These developments became particularly relevant for the design of novel coatings in the field of surface engineering.

2. COATINGS

The surface of a component is usually the most important engineering factor. While it is in use it is often the surface of a workpiece that is subjected to wear and corrosion. The complexity of the tribological properties of materials and the economic aspects of friction and wear justify an increasing research effort. In industrialized countries some 30% of all energy generated is ultimately lost through friction. In the highly industrialized countries losses due to friction and wear are put at between 1 and 2% of gross national product. To an increasing degree therefore, the search is on for surface modification techniques, which can increase the wear resistance of materials. Unfortunately, there exists an almost bewildering choice of surface treatments that cover a wide range of thickness. The choice has to be such that the surface treatment does not impair too much the properties of the substrate for which it was originally chosen; that is to say, it should not reduce the load-bearing overlooked capabilities, for example. This aspect of the substrate has been overlooked frequently in surface engineering, with emphasis put rather more on the protective coating itself. Equally, the surface treatment chosen should be suitably related to the problem to be solved.[2,3] If a thin protective layer may do the job, it does not make much sense in concentrating on processing of a thick layer on top of a substrate. It is worth noting here that wear resistance is a property not of materials but of systems, since the material of the workpiece always wears against some other medium. It is its relation to its environment (e.g., lubrication and speed of sliding/rotation) that determines the wear resistance of the material in a given construction. As a general rule, wear is determined by the interplay of two opposing properties: ductility and hardness. Wear can be reduced by modifying the surface layer in such a way that it acquires higher ductility, so that greater plastic deformation can occur without particles breaking off. Soft surface layers can be very effective in reducing wear due to delamination. Resistance to wear by abrasion, on the other hand, is then low. However, wear can also be reduced by making the surface layer harder. Then again, increasing hardness also means an increase in the elasticity strain limit and a reduction in ductility, leading to a lowering of fatigue resistance and hence to brittle failure. The characteristics of the system (i.e., whether the wear

is caused by delamination or abrasion) determine which of the surface engineering methods should be chosen. An interesting approach is decreasing the grain size, which could lead to both an increase in mechanical strength and fracture toughness.

The enormous advantages for materials properties by decreasing the grain size down to the nanometric level were very rapidly extended into the field of mechanical applications. The enthusiasm to manipulate the structure of the deposited films by playing with the binomial feature size/phases distribution was contagious. The deposition of metastable phases either of high-temperature type or with extreme shifts far from stoichiometric chemical composition led to unexpected phases, quasi-amorphous structures, and nano-sized grains. In fact, the knowledge transfer from bulk materials to coatings led to extensive studies on ceramic materials, in particular oxides, carbides, and nitrides, due to their excellent performance concerning very high hardness, chemical and thermal stability, and, in many cases, good tribological characteristics. These coatings are known as "hard coatings". Traditionally, the term *hard coatings* refers to the property of high hardness in the mechanical sense with good tribological properties, although it can be extended to other areas (optical, optoelectronics) where a system operates satisfactorily in a given environment.[4] Although for a long time, hardness has been regarded as a primary material property affecting wear resistance, the elastic strain to failure, which is related to the H/E ratio, is a more suitable parameter for predicting wear resistance.[5] The parameter H refers to hardness and the parameter E represents the Young's modulus. Within a linear elastic approach, this is understandable according to the relations that the yield stress of contact is proportional to (H^3/E^2) and the equation $G_c = \pi a \sigma_c^2/E$, with a being the crack length and σ_c the critical stress at failure. It indicates that the fracture toughness of coatings defined by the so-called critical strain energy release rate G_c would be improved by both a low Young's modulus and a high hardness.

Immediately after the first results on hard coatings, it was concluded that their final properties were outstanding compared to the corresponding bulk materials with similar chemical compositions. Among the several suggested explanations for the difference in this mechanical performance, the much lower grain size was the preferred one. However, most of the time, only empirical relationships were established without any deep understanding of what was going on. The well-known Hall–Petch relationship was frequently applied, without a critical sense that could comprise all the other cases where such a relation was not respected. This period coincided with the first steps in systematic studies in nanocrystalline materials.

Roughly speaking surface modification techniques fall into two groups[6]:

- *Processes for applying protective coatings*, e.g., plating, electrolytic galvanization, physical vapor deposition (PVD), chemical vapor deposition (CVD), and laser cladding.

- *Processes designed to modify the material of the existing surface* by altering its structure or composition. Recent developments in structural manipulation comprise laser hardening, electron beam hardening, and shot peening, whereas thermochemical treatments include nitriding, boriding, carburizing, and ion implantation.

There are two main reasons that provided an impetus for bridging the fields of nanostructured materials and coatings: (1) in various coating systems deposited by PVD or CVD, the final structures consist very often of grain sizes much smaller than obtained with traditional processing techniques; (2) the versatility of deposition techniques allows the production of materials over a large range of chemical compositions, structures, and functional properties. Many of the difficulties in processing nanocrystalline bulk materials (such as fully dense microstructures), control of phase distribution, and control of grain size and its homogeneity can be easily overcome with deposition techniques.

3. CHALLENGES AND OPPORTUNITIES

3.1. Wear: The Role of Interfaces in Nanostructured Materials

Making an appropriate microstructure of a nanostructured coating is an epitome in materials design. This is so because the concentration of lattice defects and the details of the numerous interfaces, including the topology of the triple junctions between the interfaces, determine the overall mechanical response. The overarching challenge is therefore the design of a nanostructured coating that is free of defects that degrade the structural and functional behavior. As will be discussed in various chapters in this book, from experimental and theoretical analyses, one can conclude, with a certain confidence, that deformation in nanocrystalline materials, in particular metals, is at least partially carried by dislocation activity for grain sizes above a critical value around 10–15 nm. Below that critical value, plastic deformation is mostly carried by grain boundary processes. Nevertheless, in many investigations it has been overlooked quite often that several deformation processes might act simultaneously. This means that even though dislocations are observed above the critical grain size and less below the critical grain size, various grain boundary processes are likely to occur at the same time. In evaluating the performance of a nanostructured coating, it is essential to examine the defect content as well as the microstructural features,[7,8] in particular, grain-size dispersion, distribution of interface misorientation angles, and internal strains. It can be anticipated that control of the grain-size dispersion is extremely important in the experimental design of these nanostructured coatings. A nanostructured material with a broad grain-size dispersion will exhibit a lower overall flow stress than a material with the same average grain size but with a much smaller grain-size distribution. Consequently, experimental control over the grain-size distribution is important to investigate concepts in materials design of nanostructured coatings.

Diffusion-, time-, and temperature-dependent processes play an important role in nanocrystalline materials.

In the materials design of a coating for specific mechanical applications, i.e., hard versus tough,[9–21] one has to make a distinction between crack nucleation and crack propagation. Grain-size effects can be considered as follows. Whether the material exhibits intergranular fracture can be estimated from the stress of a pileup of dislocations in a particular grain, τ^*, that is required to activate dislocations in the next grain at a distance r. The stress concentration from the dislocation pileup increases with the number of dislocations in the pileup. The latter increases with the grain size d,[22–24] and dislocation activation in the next grain occurs when

$$\tau^* = (\tau_a - \tau_0)\sqrt{\frac{d}{4r}} \tag{1.1}$$

where τ_a is the applied shear stress and τ_0 is the intrinsic, frictional shear stress, resisting dislocation motion inside the grain. Suppose that intergranular fracture occurs along the grain boundary, i.e., r in Eq. (1.1) becomes of the order of the interatomic spacing a_0, and that the effective tensile stress $\sigma^*(\cong 2\tau^*)$ becomes as large as the theoretical strength σ_{th}. The latter can be described by the decohesion of two atomic planes of surface energy γ, on which the atoms are arranged periodically. Hooke's law is assumed for the initial part of the stress–displacement curve, yielding a theoretical strength σ_{th} equal to $\sqrt{E\gamma/a_0}$. Equation (1.1) yields for crack nucleation, with $\gamma \cong Ea_0/40$,

$$\sigma_{nuc} > \sigma_0 + \frac{1}{3}E\sqrt{\frac{a_0}{d}} \tag{1.2}$$

Whether or not flow initiation is concurrent with fracture depends on the value of σ_0 in comparison with the fracture stress σ_F. When σ_0 is larger than σ_F, cracks will nucleate and the microcracks thus formed propagate along the boundary, leading to more or less brittle failure. From Eq. (1.2), it can be concluded that with decreasing grain size, the stress necessary for crack nucleation increases. The ultimate case is found in amorphous materials where crack nucleation is effectively suppressed. It does not mean that an amorphous coating would be the best choice for a tough coating because crack propagation is enhanced and purely amorphous materials are intrinsically very brittle under tension. An amorphous material shows a certain density distribution caused by localized defects having either severe shear or hydrostatic stress field components.[25] The hydrostatic stress field component, actually representing a free volume, can be annealed out but localized defects with shear stress components cannot. The latter trigger the formation of shear localization leading to enhanced crack propagation. One way of improving the materials design of an amorphous coating, keeping the suppression of crack nucleation, is to spread the localization of shear in a delocalized state by the introduction of particles in an amorphous matrix. The ductility and therefore the toughness will be enhanced provided the particles become of the same size as the width of the shear localization, i.e., $s \approx d$ in Fig. 1.1. Of course this physical picture applies

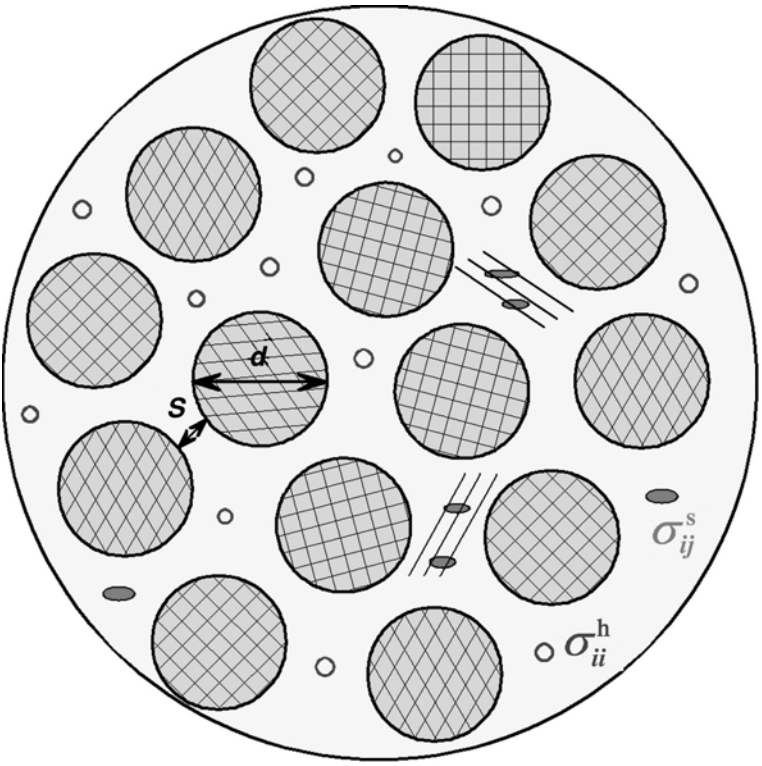

FIGURE 1.1. Nanocrystallites of diameter d separated at a distance s and embedded in an amorphous matrix. Inside the amorphous matrix, density fluctuations lead to a distribution of defects characterized by shear σ_{ij}^{s} and hydrostatic σ_{ii}^{h} stresses.

more to metallic systems than to covalent bonded amorphous materials. Although locally the mechanical response of the directionality of the bonds in amorphous carbon differs from an amorphous metal, the basic description will stay the same. For hard coatings the key challenge is to avoid grain boundary sliding, leaving grain rotation as the deformation mechanism, i.e., $s \ll d$ in Fig. 1.1. As far as toughness is concerned, more compliant (amorphous) boundary layers might be more beneficial. This was experimentally confirmed in the case of TiC/a-C:H nanocomposite coatings (Fig. 1.2). Indeed according to this physical picture, the coating with $s \approx d$ (Fig. 1.2c) showed a substantially lower wear rate compared to the situation when $s \ll d$ (Fig. 1.2a), i.e., $3 \times 10^{-17}\mathrm{m}^3/(\mathrm{N\,m\,lap})$ versus $2 \times 10^{-15}\mathrm{m}^3/(\mathrm{N\,m\,lap})$, respectively.

In most cases, as will be illustrated in the various chapters the experimental and theoretical analyses of nanostructured coatings assume that internal interfaces are free of impurities and segregation. However, segregation to interfaces may have both beneficial and detrimental effects on the mechanical performance of

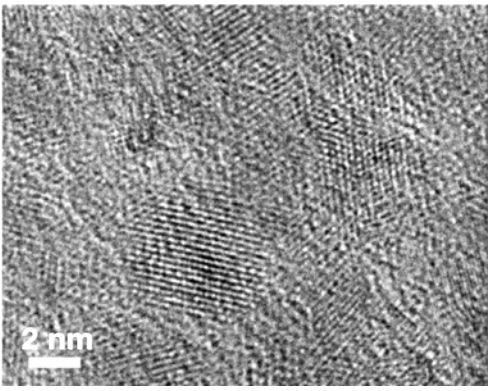

(a)

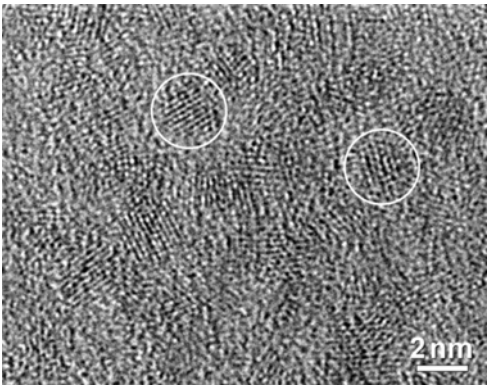

(b)

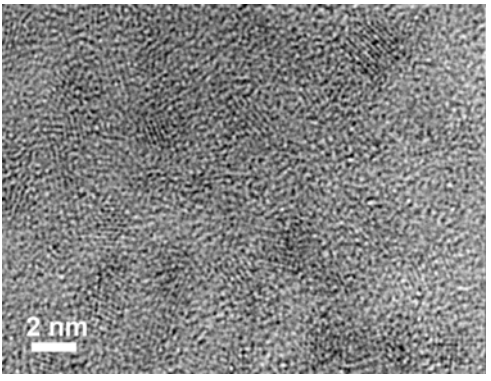

(c)

FIGURE 1.2. HRTEM micrographs showing TiC nanocrystallites embedded in an a-C:H matrix in nc-TiC/a-C:H nanocomposite: (a) $d = 4.5$ nm and $s = 0.3$ nm; (b) $d = 2.2$ nm and $s = 0.7$ nm; and (c) $d = 2.2$ nm and $s = 1.8$ nm, where d is the mean particles size and s is the mean particle spacing.

coatings. The importance of segregation to interfaces is determined primarily by the inherent inhomogeneity of interfaces, i.e., the fact that physical and chemical properties may change dramatically at or near the interface itself. The accumulation of impurity atoms at grain boundaries and surfaces leads to the formation of a very narrow zone, of the order of a few lattice spacings, with different chemical compositions. As a result of sharp concentration gradients, an isotropic bulk solid may change locally into a highly anisotropic medium. Very small bulk concentrations of impurity atoms can lead to significant amounts of those atoms at the grain boundary and interphase interfaces. This can drastically change the response of a material on loading and can eventually lead to brittle failure of an otherwise ductile material. Although embrittlement by impurity segregation is frequently observed, interface segregation can also have a ductilizing effect on brittle materials, depending on both impurity and matrix elements. Even small amounts of oxygen can contribute to interface embrittlement and the fracture mode of the material may change from cleavage to intergranular, with the fracture path closely following the interfaces. This behavior is typical of materials that have undergone certain types of heat treatments when impurities are present. The effect of segregation on surface and interfacial energies is well established.[26] It has been shown that the surface or interface energy is reduced by segregants and that those segregants that are highly surface active lead to the most drastic reduction. The effects of segregants on interface cohesion have been the subject of many discussions. Calculations for segregants in all matrices in the ideal solution approximation have given an indication of the influence of segregation on the interface cohesion.[27] However, an increase in cohesion cannot be related directly to a decrease in the propensity of intergranular fracture. The temperature at which fracture takes place may influence the fracture process. Effects of segregation on mechanical properties can be presented within a thermodynamic framework,[28] where the embrittlement of grain boundaries by solute segregation is formulated in terms of the ideal work of interfacial separation $2\gamma_{\text{int}}$. The control of γ interfacial separation

$$2\gamma_{\text{int}} = (2\gamma_{\text{int}})_0 - \left(\Delta G^0_{\text{int}} - \Delta G^0_{\text{FS}}\right) \Gamma \tag{1.3}$$

where $(2\gamma_{\text{int}})_0$ is the work of separation of a fully clean interface and Γ is the excess interfacial solute coverage (concentration per unit area), is the most appropriate way of enhancing interfacial resistance to fracture. ΔG^0_{int} and ΔG^0_{FS} are usually negative and represent the free energies of segregation to the interface and free surface, respectively, evaluated at the same temperature. Embrittlement (or ductilization) by solute segregation can now be explained with Eq. (1.3) in terms of $2\gamma_{\text{int}}$: a segregating solute with a greater free energy of segregation to a free surface compared with ΔG^0_{int} (i.e., more negative) will embrittle because $2\gamma_{\text{int}}$ will be reduced. In contrast, a lower free energy at an interface compared with ΔG^0_{FS} will enhance interfacial cohesion, i.e., $2\gamma_{\text{int}}$ increases. However, even more important than these brittle fracture modes is the effect of segregation on the ductile–brittle transition temperature (DBTT). Above that temperature a material is ductile, whereas it becomes brittle when the temperature decreases below the

DBTT. An otherwise ductile material becomes brittle because the DBTT is raised. The effects of segregants have been reported generally as variations in DBTT, i.e., δDBTT, associated with a variation in solute coverage, $\delta\Gamma$:

$$\delta\text{DBTT} \propto \delta\Gamma \tag{1.4}$$

According to Eq. (1.3) solute segregation influences the DBTT via the effect on $2\gamma_{\text{int}}$ and

$$\frac{\delta\text{DBTT}}{\delta\Gamma} \propto \left(\Delta G^0_{\text{int}} - \Delta G^0_{\text{FS}}\right) \tag{1.5}$$

In some cases, the DBTT has been observed to be inversely related to the impact fracture toughness, K_{IC}, and K_{IC}^{-1} versus Γ should be approximately linear.[29] When there is no redistribution of the segregants, the reduction in the ideal work of fracture, namely

$$\Delta 2\gamma_{\text{int}} = -\int_0^{\Gamma_{\text{GB}}} \left\{ \left[\frac{\delta G_{\text{GB}}(\Gamma)}{\delta n_i}\right]_{P,T,n_j} - \left[\frac{\delta G_{\text{FS}}(\Gamma)}{\delta n_i}\right]_{P,T,n_j} \right\} \mathrm{d}\Gamma \tag{1.6}$$

where $\left[\frac{\delta G(\Gamma)}{\delta n_i}\right]_{P,T,n_j}$ is the chemical potential of solute n_i in equilibrium with Γ at the boundary or free surface, leads in the dilute limit to Eq. (1.3). Segregants may offset the total embrittling effect described by Eq. (1.5) because of their contribution to the ease of dislocation emission at the crack tip.

It is quite obvious that all these processes at the interface have to be understood in order to tailor nanostructured coatings with a desirable set of physical and chemical properties for structural applications. The impossibility in many cases of demonstrating, experimentally, the theories that could support the particular characteristics and properties of nanocrystalline materials constituted the driving force for the huge amount of research work on the modeling of the deformation response of these materials when externally loaded. Molecular dynamics (MD) modeling has been very instrumental in the understanding of mechanical deformation mechanism of such materials, which are not accessible by experimental means.[30,31] Expressions such as "grain boundary sliding," "grain boundary diffusion," "inverse Hall–Petch relationship," "triple junctions," and "disclinations" now make part of the current terminology in our field.[32] These efforts are being directed, not only to the complete understanding of the more simple metallic materials, but also to much more structurally complex materials such as those of ceramic type. Unfortunately, the extrapolation of the knowledge already concerning nanocrystalline metals to ceramic materials is still in a very embryonic state.

3.2. Friction: Size Effects in Nanostructured Coatings

Challenging experimental and theoretical studies that have not received much attention are size effects on friction.[33] The question is whether there is a critical size below which the friction becomes negligibly small. This holds particular pertinence

in explaining the effect of the thickness of the so-called transfer layer on the counterpart during wear and the optimal size of wear debris creating the transfer layer. In DLCs (diamond-like carbons), adhesive interactions are responsible for friction and the commonly accepted idea is that covalent bonding between unoccupied states and dangling σ bonds attributes to a high friction coefficient.[34] Of course, this will dramatically change in hydrogenated DLC films and a much lower friction coefficient is observed. In fact, this crude idea is influenced greatly by the operative environment and the friction coefficient of hydrogenated DLC films increases with 2 orders of magnitude up to 0.1 when moisture and oxygen are present. In essence a-C:H represents an amorphous network composed of carbon and hydrogen. This network consists of strongly cross-linked carbon atoms with mainly sp^2 (graphite-like) and sp^3(diamond-like) bonds. Hydrogen may either bond to carbon atoms to form H-terminated carbon bonds or stay unbonded in hydrogen reservoirs. In fact, hydrogen acts as a promoter or stabilizer of the sp^3-bonded carbon phase. It is generally speculated that the low friction of most carbon films is largely because these materials are chemically inert and consequently they exert very little adhesive force during sliding against other materials. The major friction-controlling mechanisms have been suggested as the following: (1) Build-up of a transfer film on the surface of the counterpart, which permits easy shear within the interfacial materials and protects the counterpart against wear. However, the shear strength strongly depends on the tribochemical reaction with the surrounding gases present in the contact. (2) The ability to form graphitic surface layer under most tribological conditions. The wear-induced surface graphitization of DLC films consists of two steps: first hydrogen release causes relaxations and then shear deformation promotes a graphitic structure at the surface. (3) Hydrogen passivation of the dangling carbon bonds on the surface, permitting only weak interactions between the DLC film and the sliding counterpart. The friction of DLCs can be lowered by controlling the availability of hydrogen, either through incorporating hydrogen in the films or by adding hydrogen to the surrounding atmosphere. In the absence of hydrogen measurement data, it is difficult to judge the contribution of hydrogen passivation on the reduction of friction in the case of TiC/a-C:H nanocomposite coatings. However, the effect of the transfer films are clearly revealed with the *in situ* monitoring of the wear depth (actually the thickness of the transfer films) and the simultaneous recording of the coefficient of friction curves during the tribotests, together with the microscopic observations on the wear scar of the balls as will be shown in the following.

Friction can be regarded as a conversion of translational motion of the solids, with respect to each other, into vibrational energy.[35,36] It is significant to recall that, for infinite systems, the phonon spectrum consists of a continuum of vibrational modes and phonon damping can be easily realized because, due to anharmonicity, energy can be easily transferred from one mode to the other. As a matter of course, this is not the case in a finite system in which all the modes are discrete and only a certain combination of modes can carry the phonon damping. In principle, it implies that the smaller the system, the smaller is the friction and, in the limit below

a critical size, the system becomes frictionless. Surroundings will also contribute to anharmonicity and possibilities of dissipation, but the contribution to the phonon damping is still considered to be small for smaller sized systems. In the case of nanocomposite coatings, as schematically displayed in Fig. 1.1, we are facing density fluctuations that can be described as a distribution of stress fields having different character. In fact, the phonons are scattered by anharmonicities due to the strain field of these defects. In this mechanism, a translational motion interacts with phonons via scattering accompanying momentum transfer. The starting point in our description is therefore the total momentum of the phonon gas,

$$\vec{p} = \sum \hbar \vec{k} N(\vec{k}) \tag{1.7}$$

where $N(\vec{k})$ is the number of phonons in a vibrational mode $\{\vec{k}\}$. Because of the interaction, phonons are interchanged between the various modes, which leads to a variation of the occupation number $N(\vec{k})$. The average retarding force is then

$$\vec{f} = -\sum \hbar \vec{k}\, \dot{\overline{N}}(\vec{k}) \tag{1.8}$$

The rate of change of the average numbers of phonons $\overline{N}(\vec{k})$ in mode $\{\vec{k}\}$ can be expressed in a general form[37]

$$\dot{\overline{N}}(\vec{k}) = \sum W(\vec{k}, -\vec{k}')[\overline{N}(\vec{k}') - \overline{N}(\vec{k})] + \cdots \tag{1.9}$$

The sum in Eq. (1.9) represents the increase per unit of time of the average number of phonons in mode $\{\vec{k}\}$, and $W(\vec{k}, -\vec{k}')$ is the probability rate for the scattering of a phonon from mode $\{\vec{k}\}$ to $\{\vec{k}'\}$. Next, we assume, for the sake of simplicity, that the energy of the phonon gas is also conserved in three-phonon collisions, and $W(\vec{k}, -\vec{k}', -\vec{k}'')$ vanishes.

For static defects one finds, according to Fermi's golden rule,

$$W_{\text{static}}(\vec{k}, -\vec{k}') = w_{\text{static}}(\vec{k}, -\vec{k}')\delta(\omega(\vec{k}) - \omega(\vec{k}')) \tag{1.10}$$

with

$$w_{\text{static}}(\vec{k}, -\vec{k}') = 2\pi \left[\frac{(2\pi)^3}{\Omega_0 \rho_0}\right]^2 \frac{|V_1(\vec{k}, -\vec{k}')|^2}{\omega(\vec{k})\omega(\vec{k}')} \tag{1.11}$$

The δ function in Eq. (1.10) means that the energy of the phonons is conserved in collisions with *static* defects. W contains the basic physics of the description by V_1, which is the coupling between the vibrational modes, represented by $\{\vec{k}\}$, their polarization vectors $\vec{e}\,(\vec{k})$, and the defects (see Fig. 1.1), which are represented by the Fourier transforms $\Im(\varepsilon)$ of their strain fields ε. A typical element of V_1 has the form

$$V_1 = A_1(\vec{e} \cdot \vec{k})(\vec{e}' \cdot \vec{k}')\, \Im(\varepsilon)(\vec{q}) + \cdots \tag{1.12}$$

with $\vec{q} = (q_1,\ q_2,\ q_3)$. V_1 vanishes unless $\vec{k} + \vec{k}' + \vec{q} = 0$, meaning that the momentum of the phonon is changed in collisions with the defects.

In our case of a *uniformly moving* system, a standard, time-dependent, perturbation treatment yields the probability rate

$$W_{\text{moving}}(\vec{k}, -\vec{k}') = w_{\text{moving}}(\vec{k}, -\vec{k}')\,\delta(\omega(\vec{k}) - \omega(\vec{k}') - (\vec{k} - \vec{k}') \cdot \vec{v}) \tag{1.13}$$

The latter reflects in the δ function [compare Eq. (1.10)] that after the interactions not only the *momentum* changes, but also the *energy*. We assume that the time the system needs to travel a distance of the order of the phonon mean free path is *large* compared to the phonon relaxation time; i.e., the phonon distribution is then, on average, equal to the distribution in thermal equilibrium. The phonon relaxation time τ_{phonon} can be estimated from the thermal conductivity $K = c_{\text{V}}\rho v l/3$, with c_{V} being the specific heat and ρ the material density. For v we take the maximum shear wave velocity equal to $\sqrt{\mu/\rho}$, where μ is the shear modulus. Considering DLC amorphous carbon with $K = 1$ W/(m K), $c_{\text{V}} = 0.8$ J/(g K),[38,39] $\rho = 1.8 \times 10^6$ g/m^3, the phonon mean free path becomes $l_{\text{C}} \cong 0.5$ nm, yielding a relaxation time $\tau_{\text{phonon}} = l_{\text{C}}/v \cong 10^{-13}$s. The thermal conductivity of the composite can be calculated based on an effective medium theory,[40,41] but in the present case with a volume fraction of 20% of TiC it leads to a small deviation in τ_{phonon} [the thermal conductivity approaches 2 W/(m K)]. Indeed, at experimental velocities the phonon distribution is in equilibrium; i.e.,

$$\overline{\overline{N}}{}^{j}_{k} = \left[\exp\left(\frac{\hbar\omega^{j}_{k}}{kT}\right) - 1\right]^{-1} \tag{1.14}$$

where k is Boltzmann's constant and T represents the absolute temperature. If the system velocity approaches the sound velocity, the phonon distribution is *not* at equilibrium and actually a severe heat current will arise from the deviations $\overline{N}(\vec{k}) - \overline{\overline{N}}(\vec{k})$. This is basically also the difference between the thermal heat conduction that can only exist provided $\overline{N}(\vec{k}) \neq \overline{\overline{N}}(\vec{k})$ and the phonon drag that can exist even when $\overline{N}(\vec{k}) = \overline{\overline{N}}(\vec{k})$.

It is rather difficult to work out analytical equations for the phonon interactions in case the phonon distribution is not in thermal equilibrium. In general, to study the dissipative properties of a system, it is convenient to apply the quantum-mechanical technique of nonequilibrium statistical mechanics. The dissipation of energy per unit time t can be written as the product of the time derivative of the phonon Hamiltonian $H(t)$ and the deviation of the so-called density matrix, $\exp[-H(t)/T]/\text{Tr}\{\exp[-H(t)/T]\}$, from its equilibrium value. The latter can be expressed as a time-dependent integral equation and accordingly the anharmonicity drag becomes time dependent. However, in the following we will assume only interactions with a phonon gas in thermodynamic equilibrium, independent of t.

Within this theoretical framework, friction is possible only if the inverse of the phonon lifetimes are larger than the spacing of the vibrational modes.[42]

The latter depends on the size and increases with decreasing size. In a harmonic approximation, the spacing is determined by the spring constant α and the mass m. Friction will occur if

$$\frac{1}{\tau_{\text{ph}}} \geq \frac{\pi}{N}\sqrt{\frac{\alpha}{m}} \tag{1.15}$$

where N represents the number of vibrational units involved. The spring constant of C—H and C—C bonds is about 500 N/m, leading to the prediction, based on Eq. (1.15), that for N smaller than 50 unit cells, i.e., 20–30 nm, the friction becomes negligibly small. For a metal like Cu the critical thickness will be about 40 nm. It means that generating wear debris of these dimensions in the beginning is the best.

An example of the wear behavior and friction coefficient as a function of laps is shown in Fig. 1.3 for the TiC/a-C:H nanocomposite coating of Fig. 1.2c. Tribo-tests were performed on a CSM tribometer with a ball-on-disc configuration at 0.1 m/s sliding speed and 2 or 5 N normal load. The wear depth/height of the coating sample (disc) and the counterpart (6-mm-diameter ball) was monitored *in situ* with a resolution of 0.02 μm by an RVDT sensor during the tribo-tests, which allowed *in situ* measurement of the thickness of the transfer films on the surface of the counterpart in contact. The coating shows a very low steady-state friction coefficient, but also a quick drop from an initially high value of about 0.2 at the beginning of sliding until the transition point where the steady state is reached. Such a behavior is attributed to the gradual formation of a transfer film on the counterpart surface during the early stage of a tribo-test, which makes the contact in between two, basically similar, hydrophobic a-C:H surfaces that contribute to self-lubrication. Against different counterparts, i.e., sapphire, alumina, and bearing steel balls, only slight differences in the friction coefficient are observed on the coatings that self-lubricate. It may imply that the interfacial sliding actually takes place between the transfer films on the ball and the surface of the coating, rather than sliding between the surfaces of the counterpart and the coating. To prove that the self-lubrication is induced by the formation of transfer films, the wear depth was *in situ* monitored with the RVDT sensor during the tribo-tests. As marked by the arrows in Fig. 1.3, segments with a negative slope were observed in the depth versus laps graph and indicated a significant growth of the transfer film on the ball surface, rather than a real reduction in the depth of the wear track on the coatings. Correspondingly, substantial decreases in the friction coefficient were detected. The maximum growth amplitude in the thickness of the transfer films was measured at about 100 nm and the minimum at the level of 10 nm. Once the transfer film stopped growing, the coefficient of friction could not decrease further and started to fluctuate. Because the transfer film covered the ball surface in contact, the wear rate of the coating diminished at that moment and resulted in less debris formed. As a result, the transfer film became thinner with sliding distance until it broke down fully, leading to a sudden rise in the friction coefficient. Sliding at higher friction coefficient may generate more debris, which in turn provided the

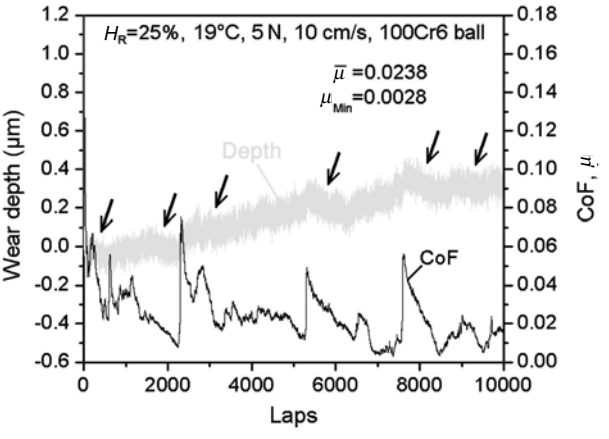

(a)

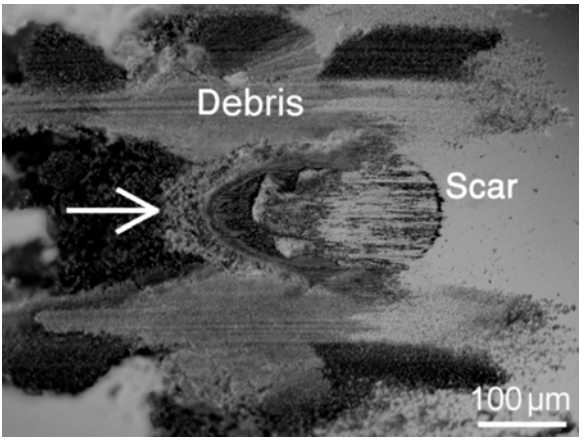

(b)

FIGURE 1.3. (a) Dynamic frictional behavior of coating sliding in air of 25% relative humidity, and (b) wear scar of 100Cr6 steel ball. (An arrow indicating the sliding direction of the coating in contact is inserted.). CoF, coefficient of friction.

necessary materials for the growth of new transfer film. Thereafter, this dynamic friction process was observed to be cyclical. Figure 1.3b shows the wear scar of the 100Cr6 ball covered with transfer films, as well as the wear debris collected in front of, and at the flanks of, the wear scar.

To understand the behavior of the coefficient of friction in the framework of size effects, the following analysis is made: For an elastic contact of a 6-mm-diameter steel ball pressed against a coating of 150-GPa elastic modulus, with a

load of 5 N, a circular contact area of 100-μm diameter will develop, corresponding to a maximum contact pressure p_0 of about 950 MPa. As a consequence of the applied load, shear stresses will develop beneath the surface, with a maximum of about 0.3-GPa shear stress 20 μm below the surface, i.e., far below the interface between the thin coating and the substrate. A typical steel substrate is able to withstand this shear stress level. The shear stress gradually decreases going toward the surface, and only low shear strength materials will be able to fail locally, with the development of debris that will ensure that a thin transfer layer will form for the reduction of friction. This is the reason why commonly lamellar, low shear strength materials such as graphite and MoS_2 are employed as solid lubricants.[43] DLC coatings suit very well this proposed framework for low friction. They are hard and stiff materials with a typically amorphous structure. A distinction must be made between hydrogenated (a-C:H) and H-free (a-C) amorphous carbons. Under contact their surface undergoes a phase transition with the local formation of aromatic structures (for a-C:H) or graphite (for a-C). These phases are characterized by low shear strengths, which will cause the formation of wear debris. Because of the low shear strength of graphitized a:C (of the order of 10–100 MPa) wear debris will be formed, the thickness of which is related to the thickness of the graphitized layer under the surface, i.e., of the order of nanometers. It leads to very low friction in agreement with the predictions based on Eq. (1.15). In the present case (Figs. 1.1–1.3) the material will yield when the contact pressure $p = \sigma_Y/\mu$, where σ_Y and μ represent the yield stress and coefficient of friction, respectively. The point of yielding is easily reached because of the low shear strength of graphitized a-C and is expected[44] to lie beneath the contact if $\mu \leq 0.3$, which is the case at the onset of the friction coefficient in the experiment (see Fig. 1.3).

Chemical effects should be considered if the influence of the atmosphere on the coefficient of friction must be explained. For a-C:H a low humidity atmosphere is the preferred condition for low friction. The H-terminated surfaces of both counterparts ensure their contact occurs under low adhesion, so that the transfer layer will be kept at the optimal thickness. The presence of humidity influences the surface properties of the counterparts, increasing their adhesion. Under these conditions the thickness of the transfer layer will vary under sliding contact, with subsequent increase of friction, which will increase wear, modifying the transfer layer thickness and leading to an unstable situation that will finally lead to high-friction sliding. For H-free a-C the situation is different, in that in this case the transfer layer formation is "dynamic," with graphite plates continuously transferring between coating and ball, because of the low shear rate along the basal planes of graphite. The ease of mutual sliding of the graphite basal planes can be improved with the presence of intercalated water molecules, giving a very different behavior as compared to a-C:H. Also in this case, when the transfer layer thickness has reached an optimum thickness there will be a stable situation, as the corresponding low friction will ensure that no further modifications of its thickness will occur. In this case sliding in vacuum or inert atmosphere leads to an

unstable high-friction state. Under vacuum sliding the p_z orbitals of each graphite atom will be dangling on the unsaturated surface, which will increase the adhesion between two such surfaces enormously, leading to high friction and wear and no possibility for transfer layer formation. Chemical effects are probably the reason why lamellar, low shear strength materials such as Ti_3SiC_2 do not exhibit low friction following the formation of a transfer layer,[45,46] which is in contrast with the classical theory of low friction, which states that a low shear strength material on top of a hard substrate is the desired low-friction configuration. To further support the theoretical framework presented here the behavior of polymers such as HDPE (high-density polyethylene) and PTFE (polytetrafluoroethylene) sliding against glass can be mentioned.[47] These polymers form a transfer layer on the hard counterpart, but their initial coefficients of friction remain around 0.2–0.3, while the transfer layers are micrometers thick. As the sliding progresses the transfer layers become much thinner, and only then coefficients of friction as low as 0.05 are measured (for PTFE).

The physical picture is that a wear debris of nanometer thickness is formed, reducing the friction according to Eq. (1.15). The wear debris is collected during the sliding process with the ball to produce a compacted transfer layer. In getting the wear debris and transfer layer in the first place the starting roughness of the ball may play a decisive role. Commonly the roughness is around 40 nm, creating high local shear stresses around the asperities that in the beginning contribute to the formation of the wear debris and the formation of the transfer layer.

3.3. Tribological Properties: The Role of Roughness

Clearly, from the last section, roughness may have a crucial influence on the attachment and detachment of layers from a substrate. Despite its importance, the effects of roughness on tribological properties have been somewhat overlooked from a research perspective in the chapters to come. Therefore, some new ideas and developments will be presented herein. This topic was studied initially by Fuller and Tabor,[48] and it was shown that a relatively small surface roughness could diminish or even remove the adhesion. In their model a Gaussian distribution of asperity heights was considered with all asperities having the same radius of curvature. The contact force was obtained by applying the contact theory of Johnson *et al.*[49] to each individual asperity. However, this approach considers surface roughness over a single lateral length scale. The maximum pull-off, or detachment, force is expressed as a function of a single parameter that determines (the statistically averaged) competition between the compressive forces from higher asperities that try to pull the surfaces apart and the adhesive forces from lower asperities that try to hold the surfaces together.

On the other hand, randomly rough surfaces, which are commonly encountered for solid surfaces,[50,51] possess roughness over many different length scales

rather than a single one. This case was considered by Persson and Tosatti[52] for the case random self-affine rough surfaces. It was shown that when the local fractal dimension D is larger than 2.5, the adhesive force may vanish or at least be reduced significantly. Because $D = 3 - H$ the roughness effect becomes more prominent for roughness exponents $H < 0.5 (D > 2.5)$. The parameter H represents the roughness exponent (not to be confused with hardness H in this chapter) that characterizes the degree of surface irregularity. Upon decreasing H the surface becomes more irregular at short length scales.

These predictions were limited to the case of small surface roughness and the calculations were performed using power law approximations for the self-affine roughness spectrum, which are valid for lateral roughness wavelengths $q\xi > 1$, with ξ being the in-plane roughness correlation length. Extension for the case of arbitrary roughness, including contributions from roughness wavelengths $q\xi < 1$, was presented in Ref. 53. Although the effect of various roughness parameters on the detachment force was partially analyzed, a more detailed study is necessary in order to provide a complete picture of the effect of various detailed self-affine roughness parameters. In the following description the rough interface either refers to the substrate/coating system or to the coating/transfer layer on a sliding ball.

We assume that the substrate surface roughness is described by the single-valued random roughness fluctuation function $h(\vec{r})$, with $\vec{r} = (x, y)$ being the in-plane position vector, such that $\langle h(\vec{r}) \rangle = 0$. The adhesive energy is given by

$$U_{\text{ad}} = -\Delta\gamma \int \mathrm{d}^2 r \sqrt{1 + \vec{\nabla} h \cdot \vec{\nabla} h} \tag{1.16}$$

Assuming Gaussian random roughness fluctuations yields after ensemble averaging over possible random roughness configuration, with γ being the surface energy,

$$U_{\text{ad}} = -\Delta\gamma A_{\text{flat}} \left\langle \sqrt{1 + \vec{\nabla} h \cdot \vec{\nabla} h} \right\rangle \tag{1.17}$$

where

$$\left\langle \sqrt{1 + \vec{\nabla} h . \vec{\nabla} h} \right\rangle = \int_0^{+\infty} \mathrm{d}u \left(\sqrt{1 + \rho^2 u} \right) e^{-u} \tag{1.18}$$

where A_{flat} is the average macroscopic flat contact area, $\rho = \sqrt{\langle (\nabla h)^2 \rangle}$ represents the average local surface slope of the substrate rough surface, and $-\Delta\gamma$ is the change of the local surface energy upon contact due to film–substrate interaction. Substituting in $\rho = (\langle |\vec{\nabla} h|^2 \rangle)^{1/2}$ the Fourier transform of the surface height $h(\vec{q}) = (2\pi)^{-2} \int h(\vec{r})\, e^{-i\vec{q}\cdot\vec{r}}\, \mathrm{d}^2\vec{r}$, with $\vec{r} = (x, y)$ being the in-plane position vector and

assuming $\langle h(\vec{q})h(\vec{q}')\rangle = \delta^2(\vec{q}' + \vec{q})\langle h(\vec{q})h(-\vec{q})\rangle$ (i.e., translation invariance), the rms local slope ρ is given by

$$\rho^2 = \int q^2 \langle |h(\vec{q})|^2 \rangle \, \mathrm{d}^2\vec{q} = \int q^2 C(q) \, \mathrm{d}^2\vec{q} \tag{1.19}$$

where $C(q)$ is the Fourier transform of the substrate height–height correlation function $\vec{r}C(r) = \langle h(\vec{r})h(0)\rangle$ that characterizes the substrate roughness. Furthermore, the elastic energy stored in the film of elastic modulus E and Poisson's ratio v is given by

$$U_{\mathrm{el}} = -\frac{1}{2} \int \mathrm{d}^2 r \, \langle h(\vec{r})\sigma_z(\vec{r})\rangle \tag{1.20}$$

assuming that the normal displacement field of the film equals $h(\vec{r})$. Since in Fourier space we have $h(\vec{q}) = M_{zz}(\vec{q})\sigma_z(\vec{q})$ with $M_{zz}(\vec{q}) = -2(1 - v^2)/Eq$[52] and $h(\vec{q}) = (2\pi)^{-2} \int h(\vec{r}) \, e^{-i\vec{q}\cdot\vec{r}} \, \mathrm{d}^2\vec{r}$, we obtain after substitution into Eq. (1.20)

$$U_{\mathrm{el}} = A_{\mathrm{flat}} \frac{E}{4(1 - v^2)} \int q C(q) \, \mathrm{d}^2 q \tag{1.21}$$

Notably, Eq. (1.21) is valid for relatively weak roughness or small local surface slopes, $\rho = \langle (\nabla h)^2 \rangle < 1$.

A wide variety of surfaces/interfaces are well described by a kind of roughness associated with self-affine fractal scaling.[50] For self-affine surface roughness $C(q)$ scales as a power law $C(q) \propto q^{-2-2H}$ if $q\xi \gg 1$ and $C(q) \propto$ const if $q\xi \ll 1$. The roughness exponent H is a measure of the degree of surface irregularity, such that small values of H characterize more jagged or irregular surfaces at short length scales ($< \xi$). This scaling behavior is satisfied by a simple Lorentzian form $C(q)$.[53] For other self-affine roughness correlation models, see Ref. 51. Simple analytical expressions of $\rho = \langle (\nabla h)^2 \rangle$ for the local surface slope yields can be derived,[53,54] and Fig. 1.4 shows calculations of the local surface slope. Clearly a strong influence of the roughness exponent H is observed.

The change in the total free energy, when the thin layer is in contact with the rough substrate, is given by the sum of the adhesive and elastic energy such that

$$U_{\mathrm{ad}} + U_{\mathrm{el}} = -A_{\mathrm{flat}} \Delta\gamma_{\mathrm{eff}} \tag{1.22}$$

where $\Delta\gamma_{\mathrm{eff}}$ is the effective change in surface free energy due to substrate surface roughness. For $\Delta\gamma_{\mathrm{eff}}$ the main roughness contribution comes from the local surface slope ρ especially at absence of interfacial elastic energy stored in the system. Moreover, since $C(q) \propto w^2$, the influence of the rms roughness amplitude w on $\Delta\gamma_{\mathrm{eff}}$ is rather simple ($\Delta\gamma_{\mathrm{eff}} \propto w^2$) for small w (for large w the contribution to adhesion is proportional to w), while any complex dependence on the substrate surface roughness will arise solely from the roughness parameters H and ξ.

Considering a uniform slab of thickness d that undergoes a displacement $\tilde{u}$ upon the action of a force F, we can calculate the necessary force F to delaminate

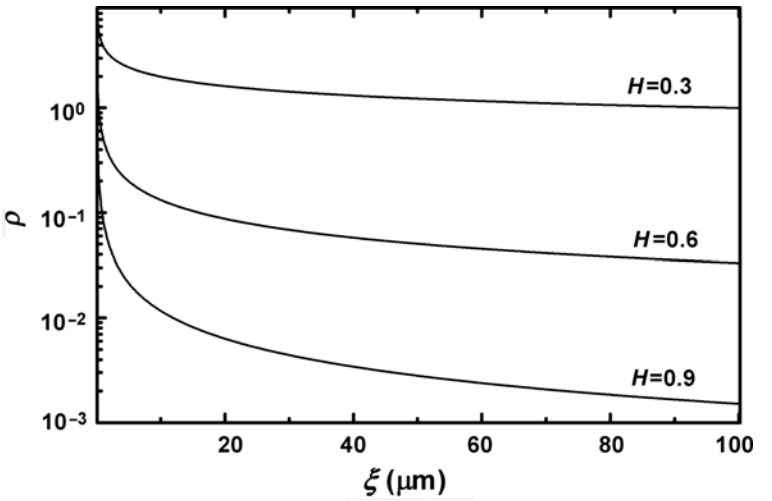

FIGURE 1.4. Local surface slope ρ as a function of the in-plane roughness correlation length ξ for $w = 10$ nm and various roughness exponents H.

the film from the substrate by equalizing the elastic energy $A_{\text{flat}} d(1/2) E(\tilde{u}/L)^2$ with the effective adhesion energy $A_{\text{flat}} \Delta\gamma_{\text{eff}}$, which is actually a Griffith calculation in fracture mechanics. Therefore, since $F = A_{\text{flat}} E(\tilde{u}/L)$, we obtain

$$F = F_{\text{flat}} \left[\int_0^{+\infty} \mathrm{d}u \, (1 + \rho u)^{1/2} \, e^{-u} - \frac{\pi E}{2(1 - \nu^2)\Delta\gamma} \int_{Q_{\text{L}}}^{Q_{\text{c}}} q^2 C(q) \, \mathrm{d}q \right]^{1/2} \tag{1.23}$$

with $F_{\text{flat}} = A_{\text{flat}}(2\Delta\gamma E/L)^{1/2}$. For small local surface slopes such that $\rho < 1$, we can rewrite the integral for the adhesive term [Eq. (1.17)] in a closed integral form and for the elastic term the analytic expression only for roughness exponents $H = 0$, $H = 0.5$, and $H = 1$ can be found.[53]

Figure 1.5 shows that the force required to detach the film increases with increasing roughness at long wavelengths or increasing ratio w/ξ, and low values of the elastic modulus E. In this case, the increment of the surface area dominates the contribution of the elastic energy. However, with increasing elastic modulus E, a maximum for the detachment force is reached, beyond which it starts to decrease rather fast and becomes even lower than the detachment force for a flat surface (elastic energy assisted detachment regime). Notably, the maximum is more pronounced for relatively low values of the elastic modulus E, so that $F_{\text{rough}} > F_{\text{flat}}$ over a significant range of roughness ratios w/ξ. The maximum indicates that the detachment can be a *multivalued* function of the ratio w/ξ, which makes the interpretation of the roughness influence more complex. The detachment force

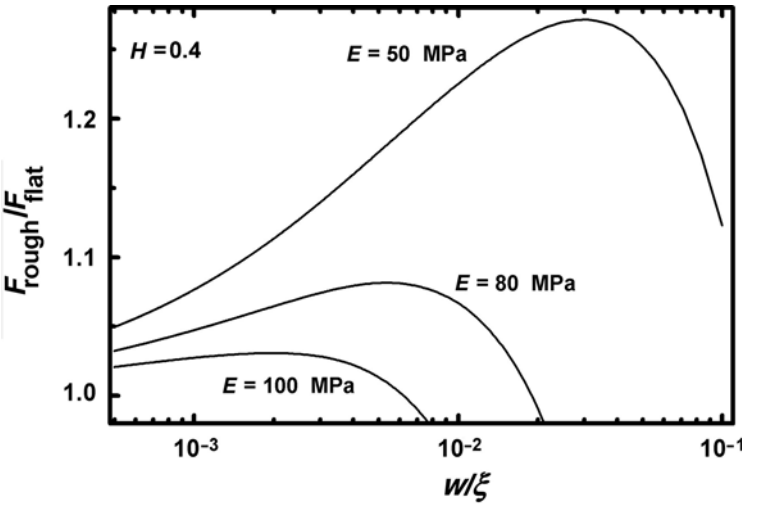

FIGURE 1.5. Detachment force $F_{\text{rough}}/F_{\text{flat}}$ versus roughness ratio w/ξ for roughness exponent $H = 0.4$, $w = 10$ nm, and various elastic moduli E.

shows a maximum with increasing roughness ratio w/ξ as long as $H < 0.5$. The detachment force decreases with increasing H at a faster rate and magnitude for $H > 0.5$ and decreasing ratio w/ξ (see also Fig. 1.6).[53,55] Up to now we assumed complete contact between the thin film and the substrate. If, however, only partial

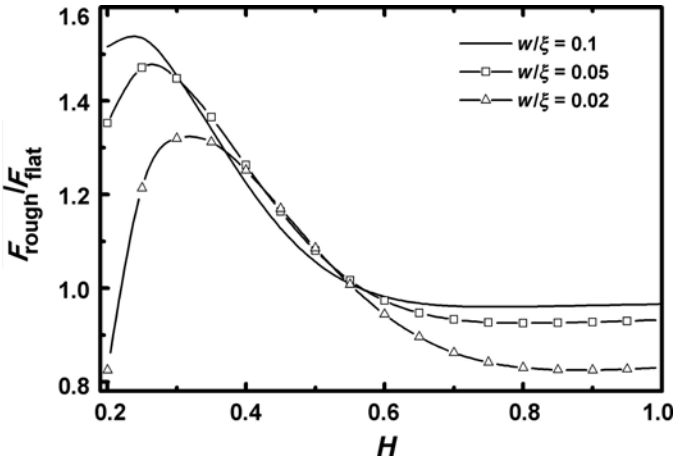

FIGURE 1.6. Detachment force $F_{\text{rough}}/F_{\text{flat}}$ versus roughness exponent H.

contact occurs at a lateral length scale λ, then the real contact area $A(\lambda)$ (if the surface was smooth on all length scales shorter than λ; or apparent area of contact on the length scale λ) is related to the macroscopic nominal contact area $A(L) = A_{\text{flat}}(\approx L^2, L \gg \xi)$.[54–56] In conclusion, it is shown that the self-affine roughness at the junction of an elastic film and a substrate influences its detachment force in a way that the detachment force can be smaller than that of a flat surface for relatively high elastic modulus E, depending also on the specific roughness details. When the surface becomes rougher at long wavelengths, i.e., with increasing ratio w/ξ, the effect of elastic energy becomes more dominant, leading to a detachment force that shows a maximum after which it decreases and becomes lower than that of a flat surface. Similar is the case of partial contact, where the detachment force also increases as the contact length increases up to a maximum for contact lengths larger than the roughness correlation length ξ. It further decreases and is followed by saturation. The multivalued behavior around the maximum further complicates the interpretation of the roughness influence. These results clearly indicate that the roughness has to be precisely quantified in fraction and wear studies. So far, we should note that our analytic calculations are strictly valid for elastic solids and more research is needed to include plasticity.

4. LEITMOTIV AND OBJECTIVE

The empirical knowledge brought by the study of many complex systems showed the importance of managing the structure of the deposited materials at different levels, including the size of the crystallites. The experience accumulated led to the development of theories based on fundamentals in materials science, which could help to explain the unusual values found for the combinations of mechanical strength and fracture toughness that some coatings could exhibit. These theories were in many cases too speculative and only very recently the use of powerful analyzing techniques is being introduced to confirm their validity. However, there are so many interrelated factors affecting the formation of a thin coating that the theories have to be progressively adapted to the arising "new" results of the characterizing experimental techniques. Without being exhaustive, and giving a simple example such as the deposition of carbon and the use of only one processing technique (e.g., sputtering), it is possible to deposit from the graphitic form up to a high degree of diamond type with sp^3/sp^2 ratios from almost 0 to almost 1 and a panoply of mechanical properties, such as hardness in the range from 1 to 80 GPa. The coatings are often deposited in a reactive mode with hydrogen contents that can reach values of 50%. The presence of other impurities resulting from the process itself, such as argon, introduces one more variable. The challenge now is to correlate all these factors, either with the microstructure (type of phases, grain sizes, phase distribution, residual stresses) or with the processing parameters (partial pressure of reactive gas, discharge pressure, input of energy in the growing film), to understand the

processing–structure–property relationships. If a ternary system is being treated, the complexity increases considerably. The possibility to form different mixtures of phases, all of them in different thermodynamic states, with several structural parameters, still justifies an empirical approximation. It must be remarked that many of the actual industrially used hard coatings belong to these ternary systems, e.g., Ti–Al–N coatings.

The synergy of knowledge acquired already by materials scientists on nanocrystalline materials and by materials engineers on the deposition and characterization of coatings is extremely important for the future development of advanced coatings. This was the leitmotiv of this book. It intends to be a text focusing on the latest developments in the interpretation of the mechanical behavior of nanocrystalline materials, in the form of both bulk and thin film. The state of the art presented in the different chapters is concentrated in the subjects that, in each field, are judged to allow being integrated in common future research studies. For materials scientists, it demonstrates a collection of experimental cases that can stimulate the interest of their unique character, in relation to the nanocrystalline nature. For the materials engineers, this book is a source of information that can bring new scents for further analysis of the experimental results. In summary, the impetus for this book revolves around the fundamental basis for the understanding of the mechanical behavior of nanostructured materials and their differences in relation to traditionally processed ones. The state-of-the-art deposition and characterization techniques for hard nanostructured coatings for mechanical applications are also proposed and reviewed.

This particular approach is quite different from the extensive literature available in both fields of nanostructured materials and hard coatings. Excellent review books, papers, and special issues of scientific journals have been published in recent years, on either the study of the mechanical behavior of nanostructured materials, supported by the results of powerful techniques of analysis, or the deposition of coatings for tribological applications by using different kinds of processing techniques, including PVD and CVD methods. Many of these references are available in the chapters of this book.

The guidelines followed for the selection of the themes were pointed on the words "mechanical behavior," in particular hardness and toughness. In all cases, special attention was paid to the relationship between the hardness and the structural/microstructural features. Two main parts can be considered in the book, the first one dealing with what can be called "fundamental principles," i.e., a close insight of the understanding of the mechanical behavior of nanostructured materials. It includes a sequence comprising bulk materials and films deposited on substrates with the necessary complement by MD simulation results for validation of the experimental results. Two main characterization techniques capable of validating the experimental microstructure–hardness relationship are also reviewed in this section. These are, namely, electron microscopy techniques with all the complementary accessories for chemical composition, bond type and structural

analyses, and depth-sensing indentation for the elastic and plastic characterization of the materials, with an emphasis on those deposited under the form of thin films. This is in most of the cases the unique suitable technique for the mechanical characterization of a coated material.

In the second part, selected hard coatings are outlined, either under development or already in industrial applications. The first restriction used in this part was the processing technique; only coatings deposited by PVD or CVD methods were considered. Furthermore, taking into account the importance of the microstructure–structure/hardness relationship in nanostructured films for the aim of this book, no contributions on intrinsically super-hard coatings were selected. Boron nitride/carbide-based films (DLC and diamond) are not treated in this book. It should be remarked that with nanocomposite structures, very interesting results are now being obtained with self-lubricating coatings, which combine their self-lubricating character to hardness values as high as 20 GPa. Two chapters were dedicated to the influence that the addition of a third element can have in the structure and functional properties of transition metal nitrides and carbides. These materials are the most widely studied and used hard coatings since the beginning of their development in the latter part of the 1960s. These chapters point at the cases where single-phase films are deposited, although the problem of phase separation has already been touched upon. The transition metal nitrides serve as a common base in most of the other chapters. Two of them deal with nanocomposite coatings: one from the materials point of view and the other on the influence of the processing parameters required to achieve this type of nanostructure. The thermal stability and the conditions for optimizing the tribological behavior of these nanostructured coatings are treated in separate chapters. Finally, the book ends with two chapters dedicated to one particular type of nanocomposite coating—the low-period multilayers. The first of these deals with the more fundamental concepts on the interaction in multilayers, whereas the last chapter gives the "happy end" to the book, presenting an extensive review of industrial applications of these kinds of coatings, particularly for multilayer films. Galileo would have appreciated it.

ACKNOWLEDGMENTS

Financial support from the foundation Fundamental Research on Matter (Physics division Netherlands Organization for Scientific Research, The Hague), TNO Institute of Industrial Technology, the Netherlands Institute for Metals Research is gratefully acknowledged. Thanks are due to Yutao Pei, Damiano Galvan, Dave Matthews, George Palasantzas, Redmer van Tijum, Willem-Pier Vellinga, Dimitri van Agterveld, and Arjen Roos for discussions on various aspects in this chapter.

REFERENCES

1. Galileo, *Discorsi e Dimonstrazioni Matematiche* (Leyden, The Netherlands, 1635) (See also: http://galileoandeinstein.phys.virginia.).
2. K. Holmberg and A. Matthews, Coatings tribology, in *Tribology Series 28*, edited by D. Dowson (Elsevier, Amsterdam, 1994).
3. K. N. Strafford, P. K. Datta, and J. S. Gray, *Surface Engineering Practice* (Ellis Horwood, New York, 1990).
4. R. F. Bunshah, Introduction, in *Handbook of Hard Coatings: Deposition Technologies, Properties and Applications*, edited by R. F. Bunshah (Noyes Publications, New Jersey, 2001), Chapter 1.
5. A. Leyland and A. Matthews, On the significance of the H/E ratio in wear control: A nanocomposite coating approach to optimized tribological behavior, *Wear* **246**, 1 (2000).
6. T. S. Sudarshan, and M. Jeandin (eds.), *Surface Modification Technologies*, Series of the Institute of Materials, vols. 1–18 (Institute of Materials, London, 1988–2004).
7. K. J. Van Vliet, J. Li, T. Zhu, S. Yip, and. S. Suresh, Quantifying the early stages of plasticity through nanoscale experiments and simulations, *Phys. Rev.B* **67**, 104105 (1999).
8. J. R. Weertman, D. Farkas, H. Kung, M. Mayo, R. Mitra, and H. Van Swygenhoven, Structure and mechanical behavior of bulk nanocrystalline materials, *MRS Bull.* **24**, 44 (1999).
9. S. Veprek, P. Nesladek, A. Niederhofer, F. Glatz, M. Jilek, and M. Sima, Recent progress in the superhard nanocrystalline composites: Towards their industrialization and understanding of the origin of the superhardness, *Surf. Coat. Technol.* **108**, 138 (1998).
10. J. Patscheider, T. Zehnder, and M. Diserens, Structure performance relations in nanocomposite coatings, *Surf. Coat. Technol.* **146**, 201 (2001).
11. F. Vaz, L. Rebouta, S. Ramos, M. F. da Silva, and J. C. Soares, Physical, structural and mechanical characterization of $Ti_{1-x}Si_xN_y$ films, *Surf. Coat. Technol.* **108**, 236 (1998).
12. T. Zehnder and J. Patscheider, Nanocomposite TiC/a-C:H hard coatings deposited by reactive PVD, *Surf. Coat. Technol.* **133**, 138 (2000).
13. A. A. Voevodin and J. S. Zabinski, Supertough wear-resistante coatings with "chameleon" surface adaptation, *Thin Solid Films* **370**, 223 (2000).
14. J. E. Kranowski and S. H. Koutzaki, Mechanical properties of sputter-deposited titanium–silicon carbon films, *J. Am. Ceram. Soc.* **84**, 672 (2001).
15. Y. T. Pei, D. Galvan, and J. Th. De Hosson, Nanostructure and properties of TiC/a-C:H composite coatings, *Acta Mater.* **53**, 4505 (2005).
16. S. Veprek and A. S. Argon, Towards the understanding of mechanical properties of super and ultrahard nanocomposites, *J. Vac. Sci. Technol. B* **20**, 650 (2002).
17. A. Cavaleiro and C. Louro, Nanocrystalline structure and hardness of thin films, *Vacuum* **64**, 211 (2002).
18. J. Patscheider, Nanocomposite hard coatings for wear protection, *MRS Bull.* **28**, 180 (2003).
19. M. Nastasi, P. Kodali, K. C. Walter, J. D. Embury, R. Raj, and Y. Nakamura, Fracture thoughness on diamond like carbon coatings *J. Mater. Res.* **14**, 2173 (1999).
20. N. J. M. Carvalho and J. T. M. De Hosson, Microstructure investigation of magnetron sputtered, *Thin Solid Films* **388**, 150 (2001).
21. N. J. M. Carvalho, E. Zoestbergen, B. J. Kooi, and J. T. M. De Hosson, Stress analysis and microstructure of PVD monolayer TiN and multilayer TiN/(Ti,Al)N coatings, *Thin Solid Films* **429**, 179 (2003).
22. J. P. Hirth and J. Lothe, *Theory of Dislocations* (McGraw-Hill, New York, 1968).
23. J. D. Embury, Strengthening by dislocation substructures, in *Strengthening Methods in Crystals*, edited by A. Kelly and R. B. Nicholson (Wiley, New York, 1971).
24. T. H. Courtney, *Mechanical Behavior of Materials* (McGraw-Hill, New York, 1990).
25. V. Vitek, *Modeling of the Structure and Properties of Amorphous Materials* (The Metallurgical Society of AIME, New York, 1983).
26. E. D. Hondros and D. McLean, *Monograph 28* (Society of Chemical Industry, London, 1968).

27. M. P. Seah, Grain-boundary segregation and T-T dependence of temper brittleness, *Acta Metall.* **25**, 345 (1977).
28. J. R. Rice and J. S. Wang, Embrittlement of interfaces by solute segregation, *Mater. Sci. Eng. A* **107**, 23 (1989).
29. J. P. Hirth and J. R. Rice, On the thermodynamics of adsorption at interfaces as it influences decohesion, *Metall. Trans A*. 11 **9**, 1501 (1980).
30. H. Van Swygenhoven, D. Farkas, and A. Caro, Grain boundary structures in polycrystalline metals at the nonoscale, *Phys. Rev. B* **62**, 831 (2000).
31. H. Van Swygenhoven and P. M. Derlet, Grain-boundary sliding in nanocrystalline fcc metals, *Phys. Rev. B* **64**, 224105/1–9 (2001).
32. M. Y. Gutkin and L. A. Ovid'ko, *Plastic Deformation in Nanocrystalline Materials* (Springer, Berlin, 2004).
33. S. M. Hsu, Nano-lubrication: Concept and design, *Tribol. Int.* **37**, 537 (2004).
34. A. Erdimir, Design criteria for superlubricity in carbon films and related microstructures, *Tribol. Int.* **37**, 577 (2004).
35. J. B. Sokoloff, Theory of atomic level sliding friction between ideal crystal interfaces, *J. Appl. Phys.* **72**, 1262 (1992).
36. P. P. Gruner, Phonon scattering, in *Fundamental Aspects of Dislocation Theory*, edited by J. A. Simmons, R. de Wit, and R. Bullough (National Bureau of Standards, USA,1970), Special Publications 317 and 363.
37. P. G. Klemens, Thermal conductivity and lattice vibration modes, in *Solid State Physics No. 7*, edited by F. Seitz, and D. Turnbull (Academic Press, New York, 1958).
38. C. J. Morath, H. J. Maris, J. J. Cuomo, D. L. Pappas, A. Grill, V. V. Patel, J. P. Doyle, and K. L. Saenger, Picosecond optical studies of amorphous diamond like carbon: Thermal conductivity and longitudinal sound velocity, *J. Appl. Phys.* **76**, 2636 (1994).
39. A. J. Bullen, K. O'Hara, D. G. Cahill, O. Monteiro, and A. Von Keudell, Thermal conductivity of amorphous carbon thin films, *J. Appl. Phys.* **88**, 6317 (2005).
40. R. Landauer, The electric resistance of binary metallic mixtures, *J. Appl. Phys.* **23**, 779 (1952).
41. F. W. Smith, Optical-constants of a hydrogenated amorphous carbon film, *J. Appl. Phys.* **55**, 764 (1984).
42. J. B. Sokoloff, Possible nearly frictionless sliding for mesoscopic solids, *Phys. Rev. Lett.* **71**, 3450 (1993).
43. I. L.Singer, R. N. Bolster, J. Wegand, S. Fayeulle, and B. C. Stupp, Hertzian stress contribution to low friction behavior of film MoS_2 coatings, *Appl. Phys. Lett.* **57**, 995 (1990).
44. K. L. Johnson, *Contact Mechanics* (Cambridge University Press, Cambridge, UK, 1999).
45. T. El-Raghy, P. Blau, and M. W. Barsoum, Effect of grain size on friction and wear behaviour of Ti_3SiC_2, *Wear* **238**, 125 (2000).
46. T. Zehnder, J. Matthey, P. Schwaller, A. Klein, P.-A. Steinmann, and J. Patscheider, Wear protective coatings consisting of TiC–SiC–a-C:H deposited by magnetron sputtering, *Surf. Coat. Technol.* **163**, 238 (2003).
47. I. M. Hutchings, *Tribology: Friction and Wear of Engineering Materials* (Edward Arnold, UK, co-published by CRC Press, Boca Raton, FL, 1992).
48. K. N. G. Fuller and D. Tabor, Effect of surface roughness on adhesion of elastic solids, *Proc. R. Soc. Lond. A* **345**, 327 (1975).
49. K. L. Johnson, K. Kendall, and A. D. Roberts, Surface energy and contact of elastic solids, *Proc. R. Soc. Lond. A* **234**, 3018 (1971).
50. P. Meakin, *Fractals, Scaling, and Growth Far from Equilibrium* (Cambridge University Press, Cambridge, UK, 1998).
51. Y. P. Zhao, G. C. Wang, and T. M. Lu, Characterization of amorphous and crystalline rough surfaces—principles and applications, in *Experimental Methods in the Physical Science*, Vol. 37 (Academic Press, New York, 2000).

52. B. N. J. Persson and E. Tosatti, The effect of surface roughness on the adhesion of elastic solids, *J. Chem. Phys.* **115**, 5597 (2001).
53. G. Palasantzas and J. T. M. De Hosson, Influence of surface roughness on the adhesion of elastic films, *Phys. Rev. E* **67**, 021604/1–6 (2003).
54. J. Krim and G. Palasantzas, Experimental observation of self-affine scaling and kinetic roughening at submicron lengthscales, *Int. J. Mod. Phys. **B*** **9**, 599 (1995).
55. G. Palasantzas and J. T. M. De Hosson, Evolution of normal stress and surface roughness in buckled thin films, *J. Appl. Phys.* **93**, 893 (2003).
56. B. N. Persson, Elastoplastic contact between randomly rough surfaces, *J. Phys. Rev. Lett.* **87**, 11161 (2001).